Kelvin wave variability near the equatorial tropopause observed in GPS radio occultation measurements

William J. Randel and Fei Wu

Atmospheric Chemistry Division, National Center for Atmospheric Research, Boulder, Colorado, USA

Received 12 May 2004; revised 20 September 2004; accepted 29 October 2004; published 1 February 2005.

[1] Temperature fields in the equatorial upper troposphere and lower stratosphere, derived from GPS radio occultation measurements for 2001–2002, show evidence for planetary-scale Kelvin waves. These waves have a characteristic eastward phase tilt with height and typical vertical wavelengths of ~4–8 km. The Kelvin waves exhibit coherent vertical structure over ~12–25 km, with maximum amplitudes near the tropical tropopause (~17 km). The waves are often quasi-stationary near the tropopause but exhibit regular eastward propagation in the lower stratosphere (with periods near 20 days). The quasi-stationary waves modulate the climatological cold tropopause over Indonesia. The transient lower stratospheric waves show enhanced amplitudes coincident with the descending westerly shear phase of the quasi-biennial oscillation (QBO). Correlations with outgoing long-wave radiation (OLR) data show that global temperature patterns over ~12–17 km (with characteristic Kelvin wave structure) vary coherently with transient deep convection over Indonesia.

Citation: Randel, W. J., and F. Wu (2005), Kelvin wave variability near the equatorial tropopause observed in GPS radio occultation measurements, *J. Geophys. Res.*, *110*, D03102, doi:10.1029/2004JD005006.

1. Introduction

[2] A large fraction of the space-time variance in tropical zonal wind and temperature fields is observed to be associated with equatorially trapped, eastward propagating oscillations termed Kelvin waves. Kelvin waves have been observed in the equatorial troposphere and stratosphere, and are typically identified by regular eastward phase progression, maximum amplitudes near the equator, and a quadrature relationship between temperatures and zonal winds (plus an absence of perturbation meridional winds). Kelvin waves have been observed in the troposphere coupled to convection, wherein the active convective centers travel eastward, coupled to the wind and temperature fields. Such modes were first identified by *Takayabu and Murakami* [1991], and have been analyzed in observational data by *Wheeler and Kiladis* [1999], *Straub and Kiladis* [2002], and *Yang et al.* [2003]. These convectively coupled waves have typical periods of ~5–10 days, zonal wave numbers ~3–6, and eastward phase speeds of ~15 m/s.

[3] Kelvin waves are also observed to propagate vertically out of the troposphere, with enhanced amplitudes near the tropical tropopause and in the stratosphere (depending on the background stratospheric zonal winds). While these waves are also primarily forced by deep convection, they are "free" modes in the sense that they do not propagate coherently with the convective centers in the middle troposphere. Rather, the wave characteristics depend on the space-time patterns of the convective forcing, plus the structure of the background winds and temperatures into which they propagate [e.g., *Garcia and Salby*, 1987]. Such Kelvin waves in the tropopause-lower stratosphere region have been observed by radiosondes [e.g., *Wallace and Kousky*, 1968; *Tsuda et al.*, 1994; *Holton et al.*, 2001], and are characterized by periods of ~10–20 days, global longitudinal structure (zonal waves 1–2), and phase speeds of ~20–30 m/s. Both the convectively coupled and "free" Kelvin waves can significantly affect the behavior of the tropical tropopause, and have been shown to influence dehydration and cirrus formation [*Fujiwara et al.*, 2001; *Boehm and Verlinde*, 2000], ozone transport [*Fujiwara et al.*, 1998; *Fujiwara and Takahashi*, 2001] and the occurrence of turbulence [*Fujiwara et al.*, 2003] near the tropopause. Low-frequency Kelvin waves in the lower stratosphere have also been observed in satellite temperature measurements [e.g., *Shiotani et al.*, 1997; *Canziani*, 1999], although the short vertical wave structure (wavelengths of ~5–10 km) is poorly resolved by most satellite instruments. Faster planetary-scale Kelvin waves in the middle and upper stratosphere (with periods of ~5–10 days, and vertical wavelengths >10 km) are better sampled by satellites [e.g., *Salby et al.*, 1984; *Mote et al.*, 2002; *Smith et al.*, 2002].

[4] Recently, *Tsai et al.* [2004] have shown evidence for equatorial Kelvin waves in the tropical upper troposphere and lower stratosphere using temperature profiles derived from Global Positioning System (GPS) radio occultation measurements. These GPS temperature data are characterized by high accuracy (~1–2 K) and high vertical resolution (~0.2 km) over altitudes ~10–30 km, and are useful for characterizing temperature oscillations with short verti-

0148-0227/05/2004JD005006$09.00

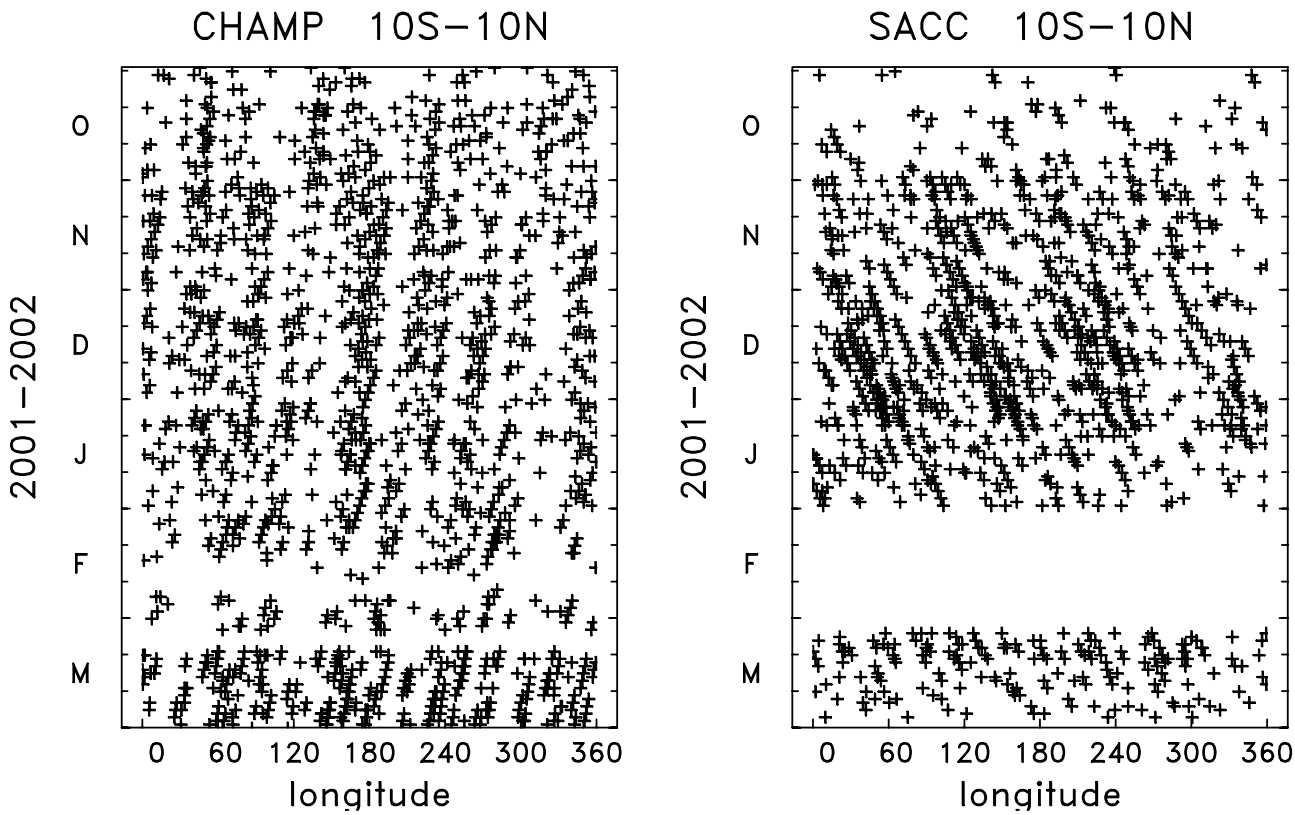

Figure 1. Plots showing the location of individual (left) CHAMP and (right) SAC-C temperature retrievals over 10°N–10°S for the period October 2001 to March 2002.

cal wavelengths (especially for gravity waves, as by *Tsuda et al.* [2000]). *Tsai et al.* [2004] use GPS measurements from the German CHAMP and Argentine SAC-C satellites during 2001–2002 to show evidence for equatorial Kelvin waves spanning the upper troposphere to lower stratosphere. This study complements and extends the analyses of *Tsai et al.* [2004] by examining the detailed time variation of Kelvin wave activity in these GPS data. Two topics of particular emphasis here are (1) how the observed Kelvin waves are influenced by the background stratospheric zonal winds, and (2) how Kelvin waves near and above the tropopause are linked with tropical deep convection.

2. Data and Analyses

2.1. CHAMP and SAC-C Data

[5] The high vertical resolution and high accuracy of GPS radio occultation temperature measurements was demonstrated by the GPS/MET satellite, which collected data during April 1995 to February 1997 [*Kursinski et al.*, 1996; *Rocken et al.*, 1997]. In this work we use GPS data from two follow-on satellite instruments, CHAMP (launched in July 2000) and SAC-C (launched in November 2000), with measurements available from both satellites since the middle of 2001.

[6] Occultation measurements from CHAMP continue to the present (early 2004), while the use of the SAC-C instrument changed after November 2002 (to focus on receiver testing). The analyses here concentrate on the time period September 2001 to October 2002, when data from both instruments are available. The temperature retrievals were processed by the University Corporation for Atmospheric Research (UCAR), but results are very similar to independent retrievals performed at the Jet Propulsion Laboratory (as used by *Hajj et al.* [2004]) and those from the GeoForschungs Zentrum in Potsdam, Germany [*Wickert et al.*, 2001]. *Hajj et al.* [2004] have extensively characterized and compared the CHAMP and SAC-C temperature retrievals, and demonstrate that individual profiles are precise to <0.6 K over 5–15 km, increasing slightly to ~2K at 25 km. The vertical resolution of GPS retrievals can approach ~100 m, but the data used here are sampled on a 0.5 km grid.

2.2. Longitudinal Gridding

[7] Under normal conditions, daily occultations from both CHAMP and SAC-C number ~200 globally. However, temperature retrievals can fail for a number of reasons, so that in practice there are ~100 temperature profiles per day. The available measurements are approximately evenly spaced in latitude, with slightly fewer near the equator. Kelvin waves are centered over the equator with a symmetric Gaussian latitudinal structure, with a typical meridional e-folding scale of ~15°–20° latitude [e.g., *Mote et al.*, 2002]. On the basis of this structure, we use all GPS measurements over 10°N–10°S for each day to analyze Kelvin wave variability. Figure 1 shows the data availability over 10°N–10°S for both CHAMP and SAC-C measurements, for the period October 2001 to March 2002. The combined sampling provides ~20–30 measurements per day, approximately evenly spaced in longitude (the detailed CHAMP and SAC-C patterns in Figure 1 are different because of

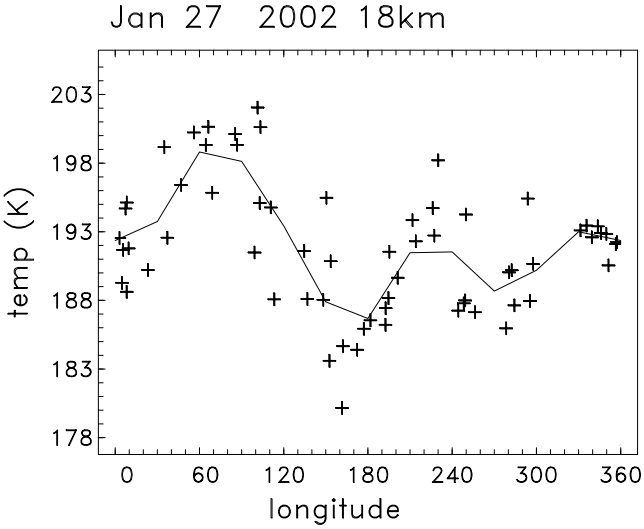

Figure 2. An example of the longitudinal gridding of GPS data for 1 day. Plus signs show individual GPS temperature measurements at 18 km over 10°N–10°S, within ±1 day of 27 January 2002. The line indicates the mapped temperature field derived from equation (1) on a 30° longitude grid.

differing satellite orbit inclinations). There are few lengthy gaps in the combined data set during September 2001 to October 2002, although one substantial gap occurs for the period over 16–24 February 2002 (this period is omitted in plots below).

[8] The data over 10°N–10°S at each altitude are gridded in longitude and time based on a simple weighted average:

$$T_{grid}(\lambda,t) = \sum_i w_i T_i(\lambda,t) / \sum_i w_i \qquad (1)$$

Here $T_i(\lambda,t)$ are the individual GPS measurements over 10°N–10°S for each day, and $w_i = \exp\left(-\left[\left(\frac{\Delta\lambda}{D}\right)^2 + \left(\frac{\Delta t}{T}\right)^2\right]\right)$ is a Gaussian weighting function in longitude and time, using D = 10° and T = 1 day. The data are gridded on a 30° longitude grid once daily, using (weighted) observations within plus and minus two days. The profile data are prescreened to remove outliers (data outside 3 sigma variance at any level over 10–30 km). Overall, this mapping provides a straightforward method to grid the irregular GPS measurements, and effectively smooths over short data voids. Tests with synthetic data show that the GPS sampling and gridding via equation (1) can accurately resolve traveling planetary waves with periods longer than ~10 days; wave periods of ~6–10 days are resolved with approximately ½ their true amplitude, while shorter periods are unresolved. The focus here is primarily on waves with periods >10 days, for which the gridding via equation (1) is well suited. Figure 2 shows an example of the GPS measurements and gridded results for one particular day (27 January 2002, at 18 km), showing a reasonable fit of the large-scale structure. Note there is considerable variability about the gridded fit, which is probably true geophysical variability given the size of the fluctuations (~2–5 K) and the precision of the GPS measurements (~1 K at 18 km). We further analyze the large-scale wave structure in the daily grids using zonal Fourier analysis; results show that zonal waves 1–2 contribute a majority of the gridded variance.

3. Results

3.1. Identification of Kelvin Waves

[9] To place the time period studied here in perspective, Figure 3 shows altitude-time sections of equatorial zonal mean temperature anomalies (deviations from the annual cycle) and zonal winds for the period May 2001 to July 2003. The temperature anomalies (Figure 3a) are derived from the combined CHAMP and SAC-C measurements,

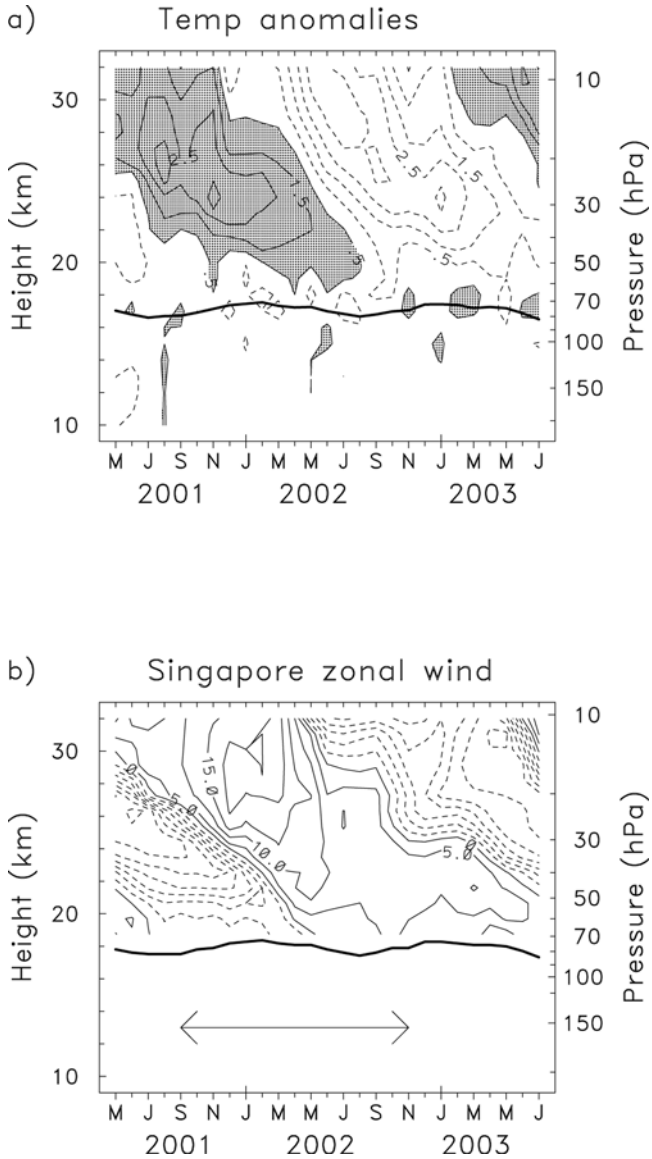

Figure 3. Height-time variations during 2001–2003 of (top) equatorial zonal mean temperature anomalies and (bottom) near-equatorial zonal winds (m/s). Temperature contours are ±0.5, 1.5, 2.5, …. The thick line near 17 km is the cold point tropopause. Temperature anomalies are derived from the combined CHAMP and SAC-C time series by removing the annual cycle at each altitude. The arrow in Figure 3b shows the time period covered by both CHAMP and SAC-C, used to study kelvin waves in the remainder of this paper.

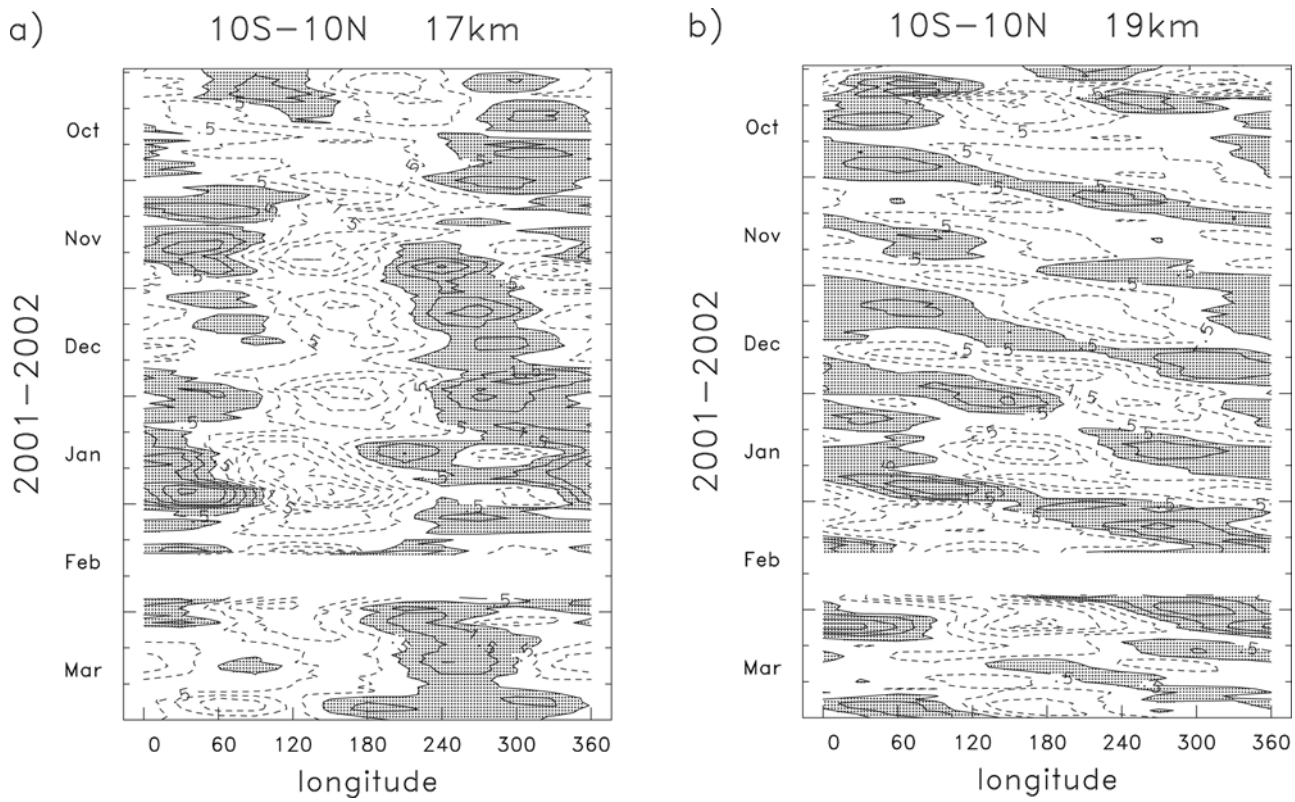

Figure 4. Longitude-time diagrams of mapped temperature variations over 10°N–10°S during October 2001 to March 2002 at (a) 17 km and (b) 19 km. Contours are ±0.5 K, 1.5 K, 2.5 K, . . . (zero contour omitted).

and deseasonalized by fitting a harmonic annual cycle at each altitude (as by *Randel et al.* [2003]). The zonal winds (Figure 3b) are from Singapore radiosonde measurements (an update of the work by *Naujokat* [1986]). Both temperatures and zonal winds show strong variability associated with the stratospheric quasi-biennial oscillation (QBO), with descending warm anomalies associated with westerly shear zones during 2001–2002, and oppositely signed anomalies in 2002–2003. The period of September 2001 to October 2002 covered by the combined CHAMP and SAC-C data (analyzed throughout the rest of the paper) occurs during a descending westerly shear phase, and previous observations have shown lower stratospheric Kelvin waves to be enhanced in QBO westerly shear [*Angell et al.*, 1973; *Maruyama*, 1991; *Shiotani and Horinouchi*, 1993]. Below we analyze the detailed Kelvin wave variations with respect to the QBO wind changes.

[10] Figures 4a and 4b show longitude-time diagrams of temperature variations at 17 and 19 km during October 2001 to March 2002, constructed from the gridded data. The 17 km level is near the tropical cold point tropopause, and Figure 4a shows the known climatological structure of cold temperatures over longitudes ~90–180°E associated with maximum convection over Indonesia [e.g., *Highwood and Hoskins*, 1998; *Seidel et al.*, 2001; *Randel et al.*, 2003]. The temperature minimum in the cold region varies episodically during these months (in response to variations in deep convection, as shown below), but overall the patterns are quasi-stationary. In contrast, temperature variations at 19 km (Figure 4b) show a zonal wave 1 structure with regular eastward propagation, and a period near 20 days (zonal phase speed of ~20 m/s). Figure 5 shows a similar diagram of the 17 km (near-tropopause) temperature variations during April–September 2002. In addition to quasi-stationary wave structure (as in Figure 4a), there are periods when eastward propagating anomalies are evident, namely during May and August–September 2002. The waves during these months have periods of ~20 days (May) and ~30 days (August–September), and there is a significant component of zonal wave 2 structure for these times.

[11] The vertical structure of temperature waves for four selected days with large wave amplitudes are shown in Figure 6. These patterns show eastward phase tilt with height (characteristic of Kelvin waves), with coherent vertical structure over ~12–25 km, and largest amplitudes near and above the tropopause (indicated by the heavy line in each panel). Note the significant depression of the tropopause altitude (by ~1 km) near 60°E in Figure 6b associated with the Kelvin wave. Vertical wavelengths near and above the tropopause during December–January (Figures 6a and 6b) are approximately 6–8 km, and this is typical for the large amplitude waves during November–March. Note that the phase lines extending into the upper troposphere in Figures 6a and 6b show more upright behavior, with correspondingly longer vertical wavelengths. Observations in May and September 2002 (Figures 6c and 6d) show shorter vertical wavelengths of ~4–5 km.

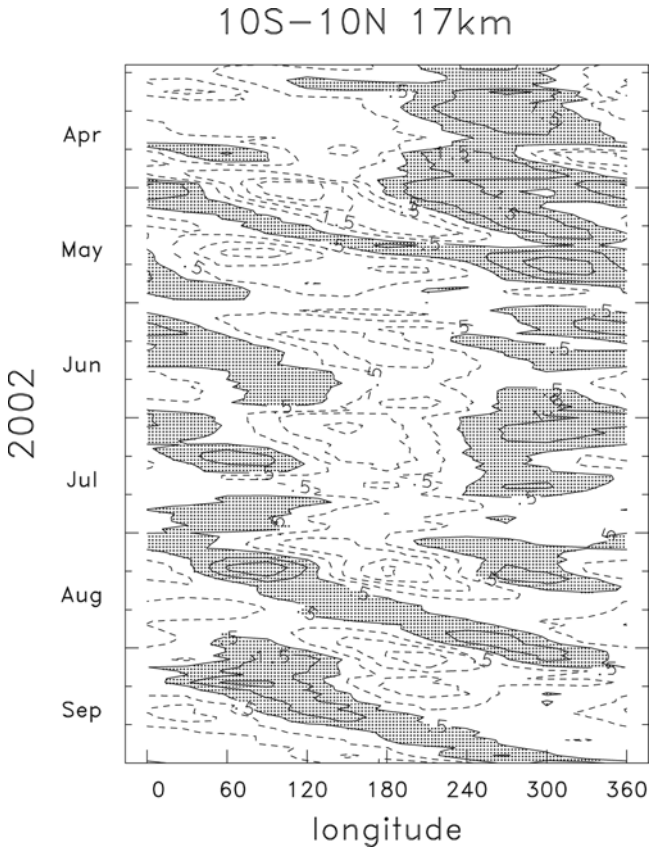

Figure 5. Same as Figure 4, but for data at 17 km during April–September 2002.

[12] The Kelvin wave event shown in Figure 6b is particularly strong, and Figure 7 shows the associated wave patterns in the original CHAMP and SAC-C temperature profiles over ~0–180°E (where wave amplitudes are largest). Here we have included measurements within ±24 hours of 28 January 2002, and simply subtracted the average background structure to highlight anomalies. The anomalies in Figure 7 show the global-scale coherence and eastward phase tilt with height characteristic of upward propagating Kelvin waves; note also that while the mapped wave structure in Figure 6b has maximum amplitudes of ~±5 K, the anomalies in Figure 7 approach 10 K in several places.

[13] Further evidence of the wave structures and validation of the GPS measurements is provided by near-coincident comparisons with radiosonde temperature measurements at Singapore (1°N, 104°E), as shown in Figure 8. Here the "full" temperature profiles and anomalies (deviations from the time average background) for GPS and radiosonde data are shown for 5 and 29 January 2002; note this latter date corresponds to the event shown in Figures 6b and 7. The anomaly vertical profiles show good agreement between the two measurements in terms of both amplitude and phase structure. This agreement is characteristic of other comparisons at Singapore during the period December 2001 to February 2002, and this prompts confidence in the global patterns derived from GPS data.

[14] The statistical behavior of Kelvin waves is often described by space-time cross-spectral analyses [e.g., *Salby et al.*, 1984]. We have analyzed the gridded GPS data following the standard wave number-frequency decomposition of *Hayashi* [1982], using overlapping 60-day time series centered on each month. Eastward traveling zonal wave number one features dominate the spectrum, and Figure 9a shows an altitude profile of wave 1 power over 12–26 km for January 2002, together with a vertical profile of the equatorial zonal winds. Figure 9a shows a strong peak for eastward traveling wave 1 with period near 20 days, and maximum amplitude over ~18–23 km (over the region of easterly zonal winds). Note that the transient wave power in Figure 9a does not extend strongly down to the tropopause level (~17 km) or below for this period, consistent with Figure 4a. There is also evidence for faster eastward waves (~10 day period) above 23 km in Figure 9a.

[15] Figure 9b shows a similar wave 1 power spectrum, but centered on May 2002. By this time the QBO easterlies have disappeared, and weak westerlies (≲10 m/s) exist throughout the lower stratosphere. Eastward waves with period ~20 days still dominate the spectrum, but wave amplitudes are confined to a narrow vertical region near and above the tropopause (~17–20 km). Note the wave phase speed ($c \sim 20$ m/s) is faster than the observed zonal winds ($\bar{u} \sim 10$ m/s), so that the waves do not reach a critical line (where $c = \bar{u}$). Spectra for August–September 2002 (a period of transience seen in Figure 5) are similar to Figure 9b, with traveling wave power for both zonal waves 1–2 concentrated in a narrow region near and above the tropopause.

3.2. Temporal Variations in Wave Amplitude

[16] The overall space-time characteristics of the planetary-scale equatorial waves in GPS data are consistent with Kelvin waves. Here we consider the detailed time variations in wave amplitudes, and their relationship to the background wind structure. Figure 10a shows height-time variations in large-scale wave variance, derived from the gridded temperature data over the entire period September 2001 to October 2002. This is calculated from the daily longitudinally gridded data (e.g., the line in Figure 2), and averaged over monthly samples. Figure 10b shows a similar plot, but for the variance associated with the residual to the gridding (e.g., the variability of the individual measurements about the line in Figure 2). For reference, Figure 10c shows the equatorial zonal wind during this time period (i.e., a subset of Figure 3b).

[17] The large-scale wave variance (Figure 10a) shows a maximum near the tropopause region, with enhanced magnitudes during December 2001 to February 2002. This variance maximum near the tropopause contrasts with the traveling wave spectra in Figure 9, which exhibit maxima somewhat above the tropopause (≳19 km); these are reconciled by the fact that quasi-stationary waves contribute much of the near-tropopause variance (e.g., Figure 4a). The residual variance (Figure 10b) also shows a maximum near the tropopause, and the residual variance magnitude is in general 2–3 times larger than the mapped large-scale variance. This is an important result, showing that small-scale features (i.e., waves not resolved in our coarse 30° longitude gridding) contribute a majority of the tropopause temperature variance in these high vertical resolution data. The residual variance also shows a clear maximum in the

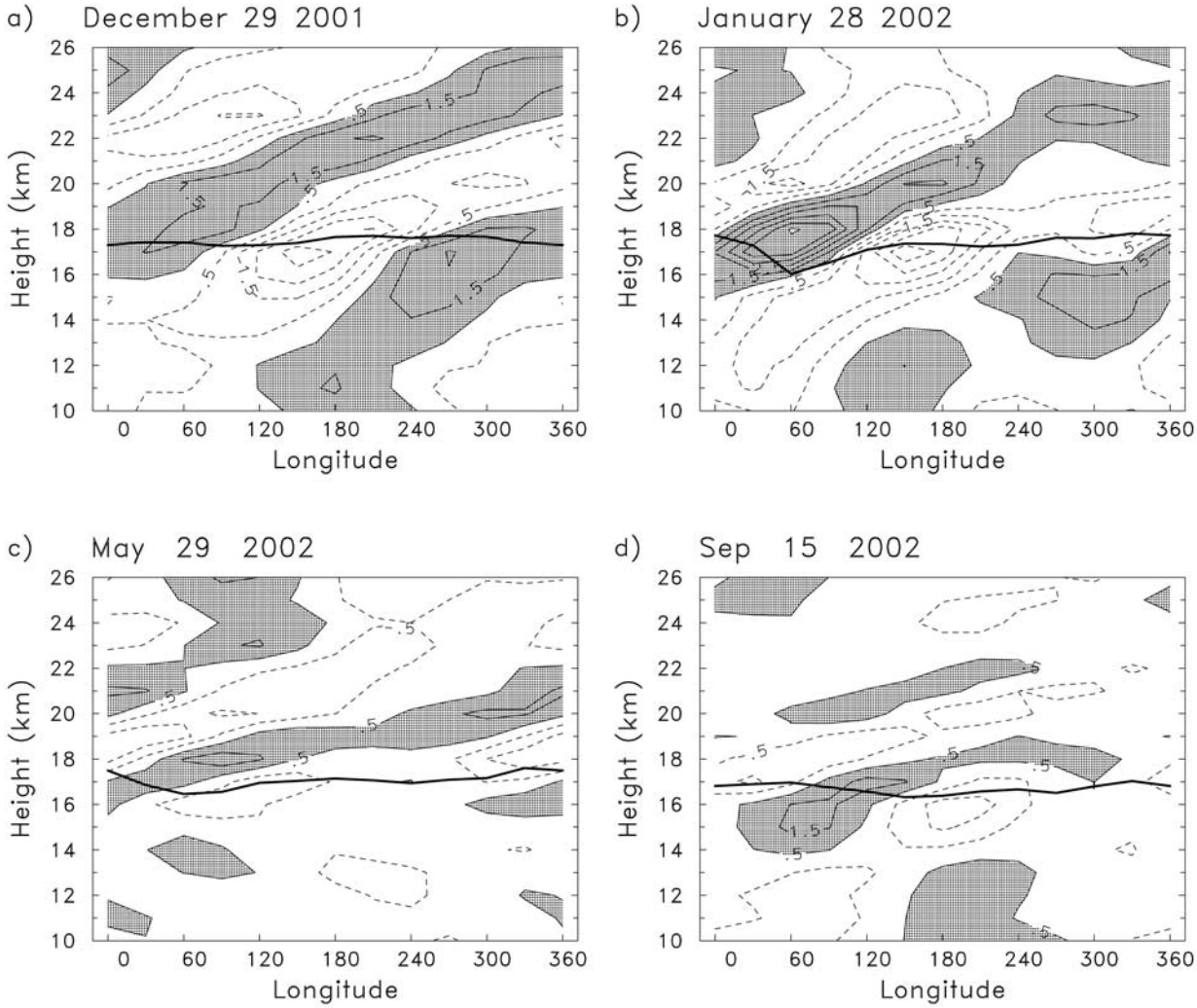

Figure 6. Height-longitude diagrams of mapped temperature anomalies over 10°N–10°S for four selected days with clear Kelvin wave structure. Contours are ±0.5, 1.5, 2.5, . . ., and the heavy line near 17 km is the cold point tropopause.

stratosphere that descends with time during September 2001 to April 2002, and closely follows the evolution of the zero line in zonal mean wind (Figure 10c). Close inspection shows a similar but weaker amplitude maximum in the mapped variance (Figure 10a). A simple interpretation of the relationship in Figure 10b is that the vertically propagating waves responsible for the temperature variations (likely small-scale gravity, inertia-gravity or other equatorial waves) interact with the zero wind line ($\bar{u} = 0$), resulting in enhanced temperature perturbations below this level (see Appendix A).

[18] Figures 11a and 11b show the detailed time variations of large-scale (mapped) and residual temperature variance over 16–23 km during September 2001 to October 2002. The large-scale variance is characterized by a high degree of transience, in terms of episodic wave maxima. These maxima are often correlated between adjacent levels, but not over the entire altitude range. Note the apparent strong influence of the ($\bar{u} = 0$) line in Figure 11a, as the large-scale wave variance at 20 km and above drops to very small values after ~April 2002. This behavior is consistent

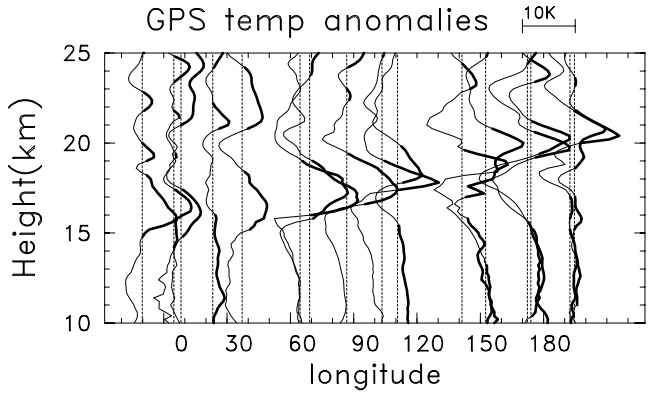

Figure 7. Vertical profiles of GPS temperature anomalies near the equator during 27–29 January 2002 (the period shown in Figure 6b). Each profile shows anomalies calculated by subtracting a background mean structure; thick lines highlight positive temperatures. Temperature scale is at top right.

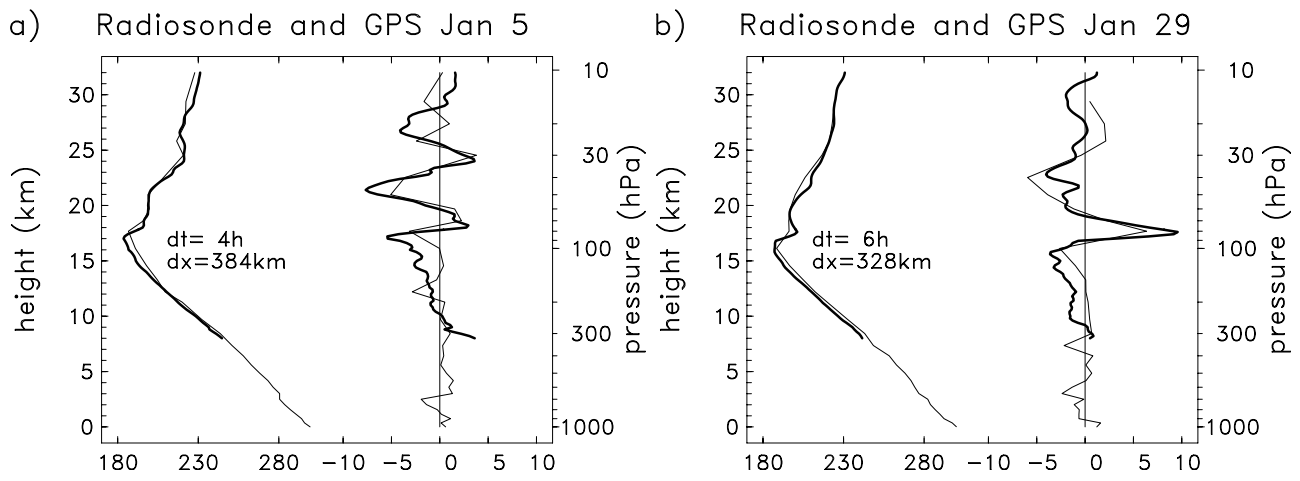

Figure 8. Vertical profiles of temperatures (left lines) and temperature anomalies (right lines) for Singapore radiosonde measurements (thin lines) and nearby GPS retrievals (thick lines). Two comparisons are shown for (a) 5 January and (b) 29 January 2002. Anomalies are defined by subtracting a seasonal mean background structure.

with the wave 1 power spectra and zonal wind changes contrasted between Figures 9a and 9b (January–May 2002). Time variations in residual variance (Figure 11b) also show episodic behavior, but they are superimposed on a larger amplitude "background" at each level (note the larger residual variance values and different vertical scales in Figures 11a and 11b). Note that the ($\bar{u}$ = 0) line has a somewhat different influence on the residual (Figure 11b) as opposed to large scales (Figure 11a), as the residual variance above 20 km does not drop to near-zero values after April 2002.

3.3. Links With Tropical Deep Convection

[19] Deep convection is a predominant source of wave variability in the tropical atmosphere [e.g., *Salby and Garcia*, 1987; *Wheeler and Kiladis*, 1999], and it is of interest to study the relationship between the large-scale Kelvin waves observed in GPS data and deep convection during the same time period. As a proxy for deep convection, we analyze outgoing longwave radiation (OLR) measurements, using the daily gridded OLR data available from the NOAA Climate Diagnostics Center website http://www.cdc.noaa.gov. These daily data are available on a 2.5° latitude-longitude grid, with data gaps filled by linear interpolation to provide complete sampling. Tropical deep convection is typically associated with OLR values below ~210 K. Figure 12 shows a longitude-time diagram of the OLR data, averaged over 10°N–10°S, for the time period October 2001 to March 2002 (identical to that in Figure 4). The most intense and variable deep convection is observed over the sector ~60°–180°E (near Indonesia), and much of the variability during this time period appears in slowly eastward propagating features (phase speeds $\lesssim$ 5 m/s) associated with the tropical intraseasonal or Madden-Julian oscillation [*Madden and Julian*, 1971]. Note that the phase speed of the traveling OLR patterns in Figure 12 is much slower than the tropopause-lower stratosphere Kelvin waves observed in Figure 4, so that the latter are not continuously coupled to convection. Rather, the observed Kelvin waves are more consistent with "free" modes forced by the broad spectrum of convective variability, especially that over the active Indonesian region.

[20] Daily variability in the intensity of convection near Indonesia is quantified in Figure 13, showing OLR averaged over 10°N–10°S and 60°–180°E for the period September 2001 to October 2002. This reveals episodic variations in convective intensity with a broad range of timescales (~20–60 days). Figure 13 also shows time series of large-scale (mapped) temperature variance at 16.5 km derived from GPS data (the same time series shown in Figure 11a). Figure 13 shows that peaks in wave variance near the tropopause are often linked with peaks in deep convection (as noted by the arrows in Figure 13), although the correspondence is not exact (e.g., the convective peak in June 2002 without a temperature wave maximum). The correlation between the time series in Figure 13 is 0.54, which is significant at the 1% level. Similar correlations between OLR and large-scale temperature wave variance are observed for all levels over 12–18 km. However, the correlations do not extend to levels above 19 km, and this is at least partly due to the strong influence of the stratospheric zonal winds on wave amplitudes seen in Figure 11a.

[21] The spatial structure of equatorial temperature variations correlated with deep convection near Indonesia is shown in Figure 14a. This shows a map of the correlations between the OLR time series shown in Figure 13 (OLR averaged over 10°N–10°S and 60–180°E) and the mapped temperature fields at each longitude and height. The calculations are made for the period November 2001 to March 2002, which is the period of strongest wave activity. Resampling calculations suggest that correlations with magnitudes of ~0.3 are significant at the 5% level. The correlation patterns in Figure 14a show a clear eastward tilting Kelvin wave structure spanning the upper troposphere-lower stratosphere, very similar to the individual day "snapshots" shown in Figure 6. These correlations with OLR demonstrate that the Kelvin waves are directly related to episodic convective forcing. Upper tropospheric

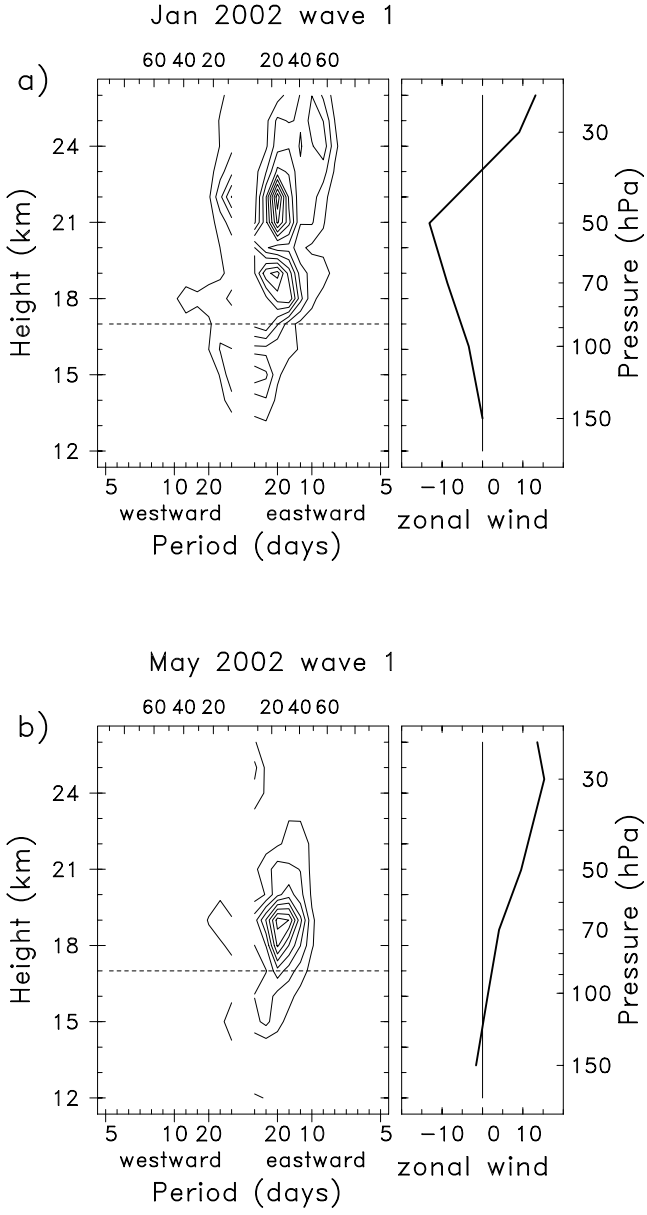

Figure 9. Altitude profiles of zonal wave number 1 space-time power spectra calculated from gridded GPS data, for 60-day time series centered on (a) January 2002 and (b) May 2002. Numbers on the top axis refer to zonal phase speed (m/s). Right panels show the corresponding zonal mean zonal winds taken from ERA40 reanalyses.

temperatures (∼10–14 km) show a dipole structure, with warm anomalies near the dateline (east of convection) and cold anomalies to the west. At tropopause level (17 km), the temperature response in oppositely signed, with cold anomalies over ∼120–210°E, and warm anomalies over ∼0–90°E. These episodic dipole variations in equatorial tropopause temperature are evident in Figure 4a. We note that the eastward tilting temperature correlation patterns in Figure 14a resemble the temperature anomalies isolated for convectively coupled Kelvin waves of *Wheeler et al.* [2000, Figure 7]. There is a substantial difference in zonal scales, however, in that the convectively coupled waves span a horizontal range of ∼100° longitude, whereas the patterns in Figure 14a are truly global scale.

[22] Figure 15 shows an example of the relation between convective forcing and global-scale temperature response near the tropopause revealed in GPS data, based on the large amplitude wave event of late January 2002 (see Figure 13). During this time deep convection occurs over longitudes ∼70–110 E and ∼140–170 E (see Figure 12), and reaches altitudes of approximately 11–13 km (based on the OLR values converted to brightness temperature, and then to height based on the background temperature field). The vertical profile of thermal forcing in these convective systems typically has a broad maximum in the middle troposphere over ∼2–8 km [e.g., *Johnson and Ciesielski*, 2000]. The mapped GPS temperatures highlight a global-scale Kelvin wave response to this forcing near and above the tropopause, with amplitudes of ∼±5 K (or larger; see Figures 7 and 8b), together with a significant modulation of the tropopause itself.

[23] The cold temperature anomalies that overly convection near and below the tropopause (∼14–17 km) in Figures 14a and 15 are consistent with cooling due to convective detrainment above the level of neutral buoyancy [*Sherwood and Dessler*, 2001; *Kuang and Bretherton*, 2004]. However, this local cooling is clearly embedded within a larger (planetary) scale temperature pattern associated with the Kelvin wave. Thus the observed temperature response to transient deep convection is consistent with both convective cooling and a global-scale response, and these may in fact reinforce each other in the tropopause region. Note that because the overall temperature response is highly nonload in space, estimates of temperature changes only colocated with convection [e.g., *Sherwood et al.*, 2003] will neglect the important far-field response.

[24] Figure 14b shows a temperature-OLR correlation map for the time period April–September 2002. Spatial patterns similar to those in Figure 14a are observed in the upper troposphere and near-tropopause level, but the correlations do not extend above the tropopause. This simply reflects the fact that the large-scale waves do not propagate into the lower stratosphere during QBO westerly winds (e.g., Figure 11a). The local cooling above convection (∼14–17 km) is again seen to be embedded in a planetary-scale structure, with implications as discussed above.

4. Summary and Discussion

[25] GPS radio occultation measurements provide high vertical resolution temperature profiles, which are useful for quantifying and understanding thermal variability of the tropical tropopause region. We have used GPS temperature profiles derived from the CHAMP and SAC-C satellites to study the variability of Kelvin waves near and above the equatorial tropopause during 2001–2002. The Kelvin waves have planetary zonal scales (zonal waves 1–2), and are identified by a characteristic eastward phase tilt with height. Vertical wavelengths of ∼6–8 km are observed near and above the tropopause in December 2001 to January 2002 (Figures 6a and 6b), while shorter vertical wavelengths (∼4–5 km) are observed in May and August–September 2002 (Figures 6c and 6d). The Kelvin wave temperature variations have (mapped) ampli-

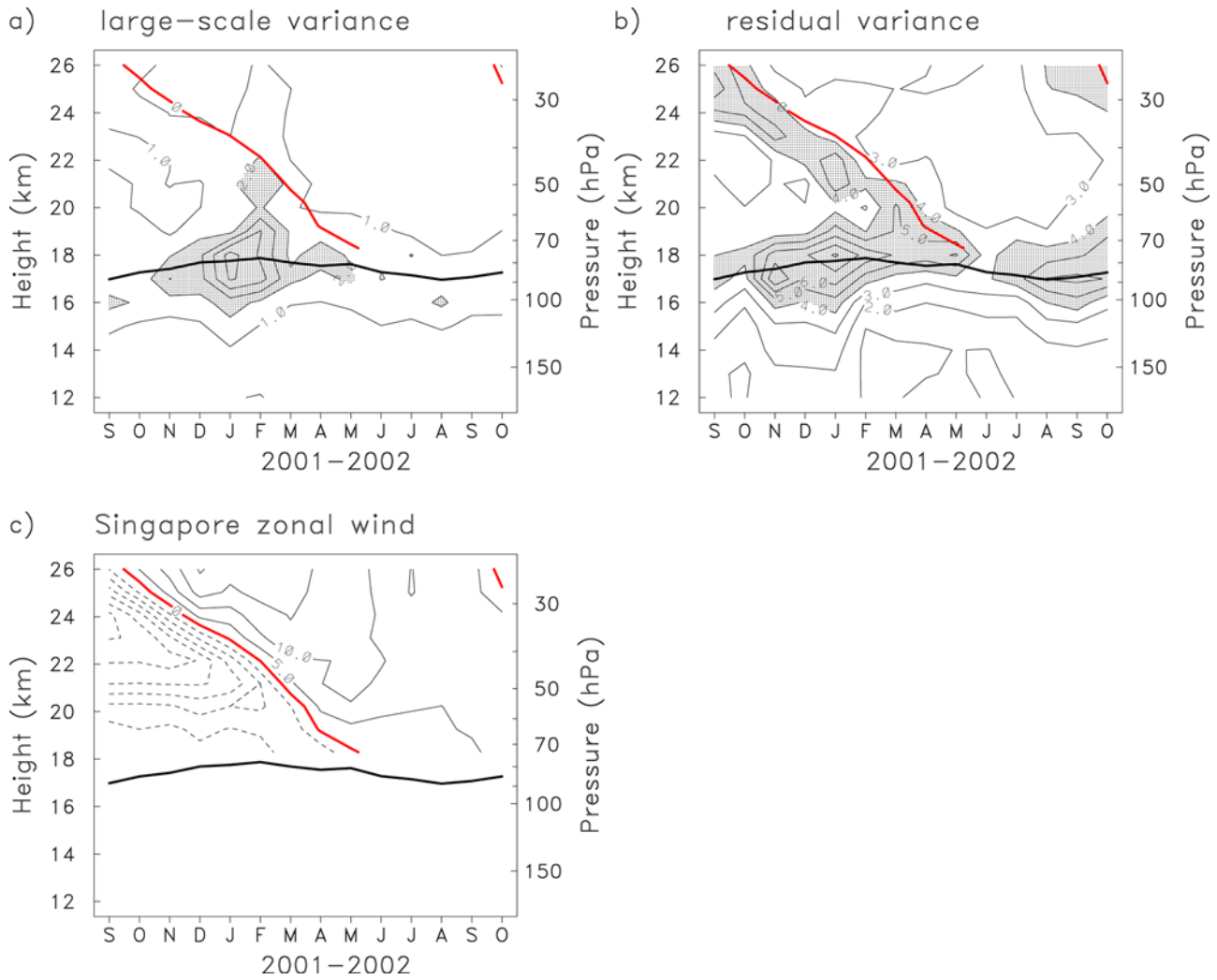

Figure 10. Height-time profiles of (a) mapped temperature variance, (b) residual temperature variance, and (c) equatorial zonal winds (m/s) derived for monthly averaged data. Temperature variance units are K^2, with values above 2 and 4 K^2 shaded in Figures 10a and 10b, respectively. The horizontal line near 17 km is the cold point tropopause, and the red line in Figures 10a and 10b corresponds to the $\bar{u} = 0$ line in Figure 10c.

tudes of ~2–4 K, but can approach 10 K in individual profiles (Figure 7). The wave structures are often quasi-stationary near the tropopause, but exhibit regular eastward propagation in the lower stratosphere (with periods near 20 days). Eastward propagation is also observed near the tropopause for several periods (May and August–September 2002). The temperature anomalies derived from GPS data are in good agreement with near-coincident radiosonde measurements (Figure 8), enhancing confidence in the global GPS structures.

[26] The combination of quasi-stationary behavior near the tropopause and eastward propagation in the lower stratosphere is consistent with the modeling results of *Garcia and Salby* [1987], who consider the atmospheric response to a broad spectrum of transient tropical convective forcing. A combination of low- and high-frequency convective forcings (e.g., the OLR variations seen in Figure 12) result in a quasi-stationary temperature response coincident with the forcing (with cooling near tropopause level), together with vertically propagating Kelvin waves above this region. The stationary wave structure near the tropopause region is also found in the modeling results of *Highwood and Hoskins* [1998]. The eastward phase tilt of the time-average temperature field near the tropopause [*Randel et al.*, 2003, Figure 6] reflects the quasi-stationary Kelvin wave patterns shown here.

[27] The traveling Kelvin waves observed in the lower stratosphere have periods ~20 days throughout the record here, while the vertical wavelength changes between 6–8 km (December 2001 to January 2002) and 4–5 km (May and September 2002). These variations in vertical wavelength are consistent with the Kelvin wave dispersion relation [e.g., *Andrews et al.*, 1987] and changes in the background zonal winds. For Kelvin waves, the vertical wave number m is related to the background flow according to:

$$m = \frac{N}{(\bar{u} - c)}. \qquad (2)$$

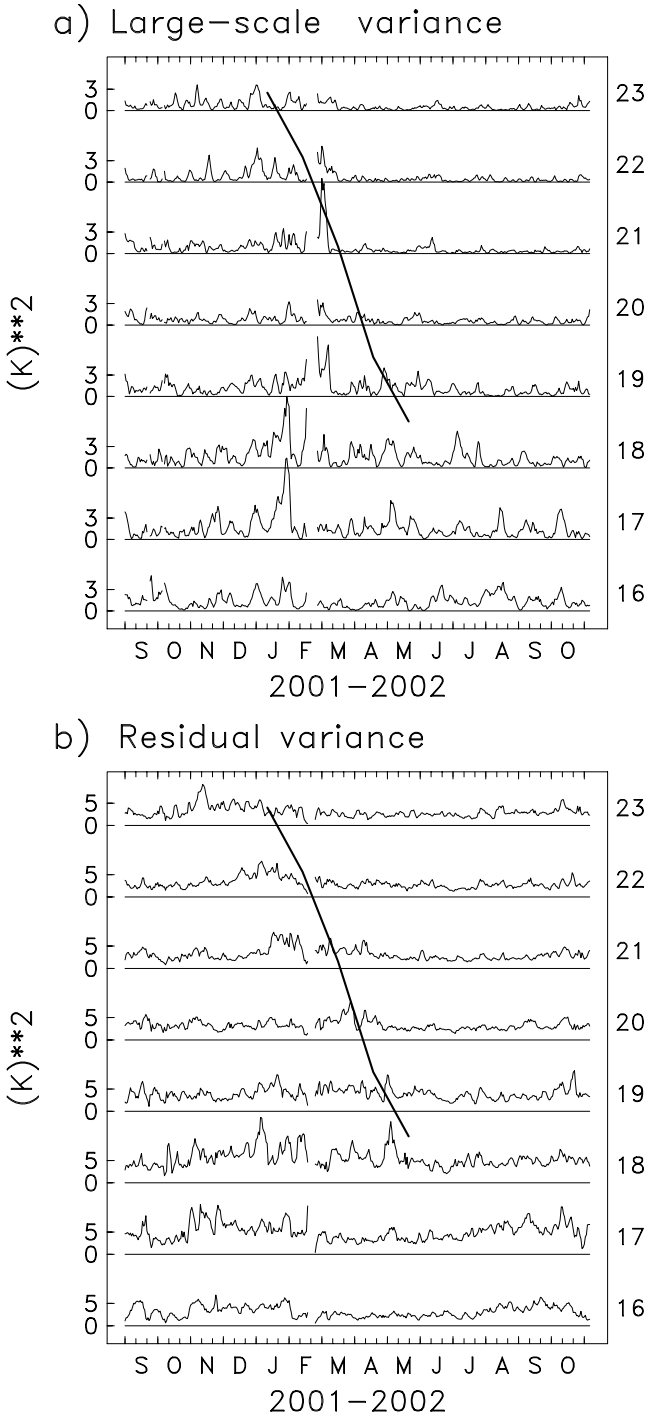

Figure 11. Time series of daily temperature variance at individual altitude levels during September 2001 to October 2002 derived from GPS data. (a) Large-scale (mapped) variance and (b) residual temperature variance; note the different vertical scales between Figures 11a and 11b. The thick sloping line corresponds to the $\bar{u} = 0$ line from Figure 10c.

Here $m = \frac{2\pi}{\lambda_z}$, with λ_z the vertical wavelength, N is the Brunt-Vaisalä frequency ($\sim 2 \times 10^{-2}$ s^{-1} in the stratosphere), $\bar{u}$ is the background zonal wind and c the zonal phase speed. For zonal wave 1 features with ~20 day period, $c \sim 20$ m/s. For the period December 2001 to January 2002 the background zonal winds in the lower stratosphere are $\bar{u} \sim -10$ m/s (Figure 9a), and this results in a calculated $\lambda_z \sim 9$ km. During May (and September) 2002, the zonal winds are ~5 m/s (Figure 9b), which gives a calculated $\lambda_z \sim 5$ km. Thus the changes in vertical wavelength seen in Figures 6a–6d are approximately consistent with observed variations in lower stratospheric zonal winds (which are in turn associated with the QBO).

[28] Previous analyses of radiosonde data [*Angell et al.*, 1973; *Maruyama*, 1991; *Shiotani and Horinouchi*, 1993; *Sato et al.*, 1994; *Canziani and Holton*, 1998] have shown that lower stratospheric Kelvin waves achieve maximum amplitudes when the background QBO winds have strong westerly shear. The GPS observations here are consistent with this: the strongest Kelvin waves are observed during November 2001 to May 2002, coincident with the descending westerly shear zone of the QBO (Figure 10). The altitude range of the Kelvin waves appears linked to the strong westerly shear zone: during January 2002 the waves extend over ~17–24 km, whereas in May and August–September 2002 a narrower vertical extent (~17–20 km) is observed (Figure 9). Virtually no planetary-scale waves are observed above ~20 km after the QBO winds change to westerlies (Figure 11a). We note that the Kelvin waves (with phase speeds of $\gtrsim 20$ m/s) do not experience a critical region

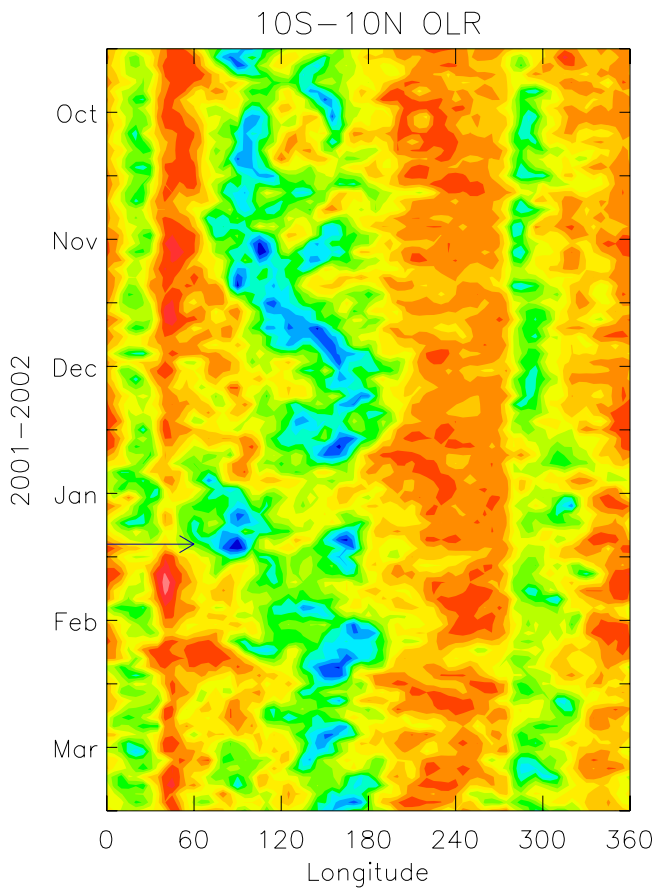

Figure 12. Longitude-time diagram of outgoing longwave radiation (OLR) over 10°N–10°S during October 2001 to March 2002 (the same time period as in Figure 4). Blue and green colors correspond to deep convection. The arrow (on 27 January) denotes the time period shown in Figure 15.

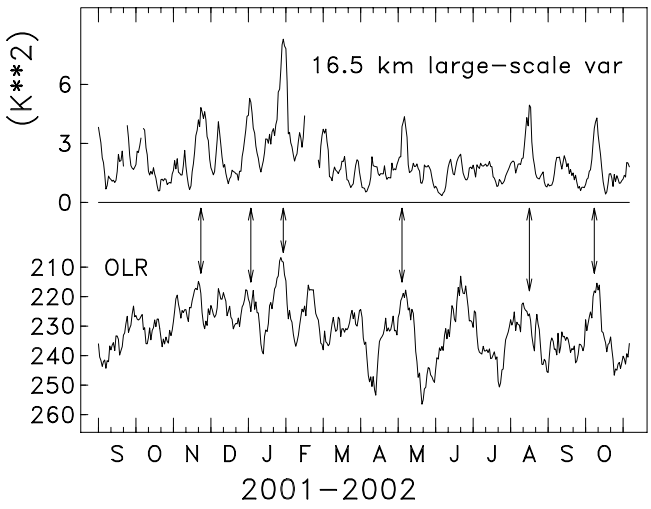

Figure 13. Time series of large-scale temperature variance at 16.5 km (top curve) and OLR averaged over 10°N–10°S, 60°–180°E (near Indonesia, bottom curve). Note the relationship between maxima in wave variance and transient convection, as indicated by the arrowed events.

(where $\bar{u} = c$; see Appendix A); the strong relationship with background winds may rather be due to thermal damping which is inversely proportional to the vertical group velocity ($Cg_z \sim |\bar{u} - c|^2$) [see *Shiotani and Horinouchi*, 1993].

[29] A large fraction of the temperature variance in the GPS measurements is associated with the residual to the large-scale mapped data (see Figures 2 and 10b). These small-scale features probably represent true geophysical variability, given the accuracy of the GPS measurements, and are likely attributable to smaller-scale waves, such as gravity or inertia-gravity waves [*Shimizu and Tsuda*, 1997; *Tsuda et al.*, 2000], or a variety of other equatorially trapped modes [e.g., *Wheeler and Kiladis*, 1999]. Enhanced amplitudes of inertia-gravity waves in the deep tropics have been observed [*Allen and Vincent*, 1995; *Tsuda et al.*, 2000] and have been explained by *Alexander et al.* [2002] as a straightforward consequence of the latitudinal variation of the Coriolis parameter. The observations here (Figure 10b) show a clear maximum in small-scale wave variance near the tropopause, and a similar temperature variance maximum near the tropical tropopause is found in the radiosonde data analysis of *Sato et al.* [1994]. *Sato et al.* [1994] furthermore show that this local variance maximum is associated with wave periods longer than ~3 days, but this does not discriminate between equatorially trapped versus inertia-gravity waves (which have periods longer than 3 days equatorward of 10° latitude). Further characterization of these small-scale temperature variations near the tropopause is important, for example for understanding the details of dehydration and cirrus formation [*Jensen and Pfister*, 2004; M. Niwano, Tenuous cloud in the tropical tropopause layer as observed by HALOE, submitted to *Geophysical Research Letters*, 2004]. The GPS data here also show an intriguing enhancement of wave variance in the lower stratosphere that descends with time in concert with the descending QBO zero wind line. The residual wave variance is a maximum approximately 1–2 km below the ($\bar{u} = 0$) line, and this maximum is qualitatively consistent with the expected behavior of gravity or inertia-gravity waves (see Appendix A).

[30] Tropical Kelvin waves are primarily forced by transient deep convection, and we have studied this relationship using global OLR data as a proxy for convective activity. Large-scale wave amplitude variations throughout the upper

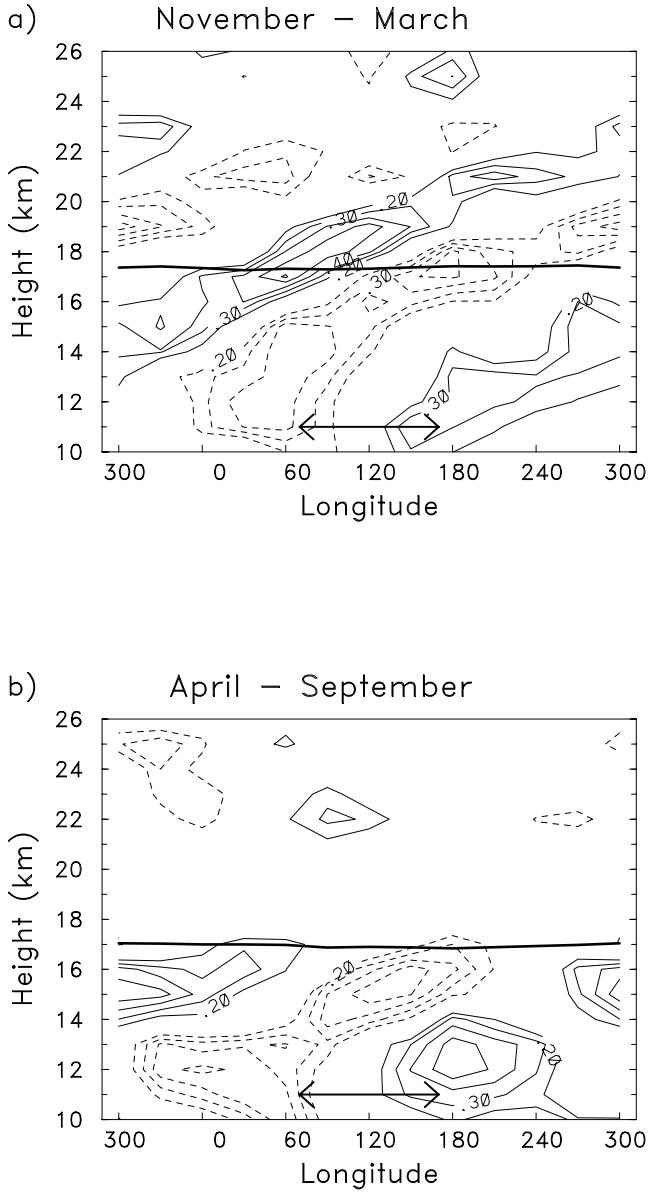

Figure 14. Correlation maps between OLR variations over 10°N–10°S, 60°–180°E (the location is indicated by the thick arrows; the time series is shown in Figure 13) and mapped GPS temperature data at each longitude and altitude. The temperature time series have been lagged by 2 days with respect to OLR to maximize the overall correlations. The sign of the correlations is such that negative (dashed) lines refer to cold temperature anomalies during enhanced convection (low OLR). Contours are ±0.2, 0.3, 0.4, …. The thick line is the cold point tropopause. Results are shown for the periods (a) November 2001 to March 2002 and (b) April–September 2002.

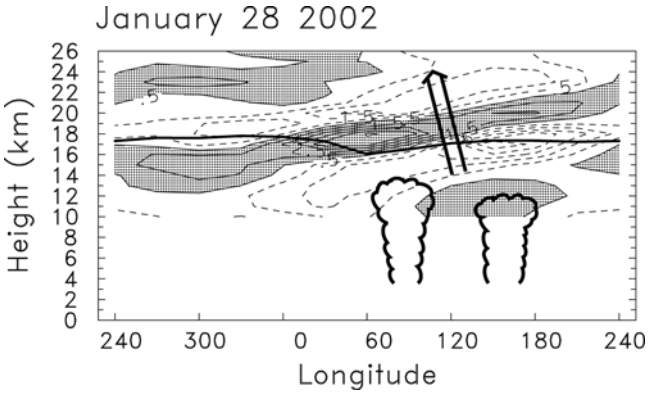

Figure 15. Diagram showing the relationship between convective forcing and Kelvin wave temperature response near the tropopause for the event in late January 2002. The location and altitude of convection is derived from OLR data (as shown in Figure 12). Contours for temperature anomalies are ±0.5, 1.5, 2.5, . . ., and the thick line is the cold point tropopause. The vertical arrow denotes the Kelvin wave group velocity (perpendicular to the phase lines).

troposphere are linked with the magnitude of transient convection near Indonesia (Figure 13). The spatial patterns of temperature correlations show a characteristic Kelvin wave structure (Figure 14), demonstrating that the Kelvin waves observed in GPS data are a response to transient deep convection. The Kelvin waves extend into the lower stratosphere when QBO easterlies are present (November 2001 to March 2002, Figures 14a and 15), whereas the response is confined mainly to the upper troposphere when the QBO is in the westerly phase (April–September 2002, Figure 14b). In both cases, transient convection near Indonesia causes a planetary-scale temperature response near the tropical tropopause, with a dipole pattern of warm and cold anomalies (with cold temperatures overlying the convection). These patterns are in good agreement with the calculated response to a broad spectrum of tropospheric convective heating [e.g., *Garcia and Salby*, 1987]. However, the cold anomalies overlying convection over ~14–17 km are also consistent with cooling due to convective detrainment above the level of neutral buoyancy [*Sherwood and Dessler*, 2001; *Kuang and Bretherton*, 2004]. Thus both of these effects (global-scale wave response and convective cooling) may contribute to the observed cooling of the tropopause region above deep convection, and may in fact reinforce each other. The global-scale temperature response to localized forcing is important to recognize in assessing the impacts of convection on the tropopause region.

Appendix A: Increase of Residual Temperature Variance Below the $\bar{u} = 0$ Level

[31] The increase in residual temperature variance in the lower stratosphere (below the $\bar{u} = 0$ level) seen in Figure 10b, and its coherent descent in time with the $\bar{u} = 0$ level, suggest an interaction between the small-scale waves and the $\bar{u} = 0$ region. Assuming that the small-scale features observed in GPS temperature data are associated with tropical gravity or inertia-gravity waves [*Tsuda et al.*, 2000], this variance increase can be attributable to two (related) processes. First, temperature perturbations associated with vertically propagating gravity waves in background shear flow have a functional dependence like $\delta T \sim |\bar{u} - c|^{-1/2}$ [*Lindzen*, 1981, equation (6)], and thus temperature variance will behave as $|\bar{u} - c|^{-1}$. For a spectrum of tropical inertia gravity waves with phase speeds centered around c = 0 [e.g., *Alexander and Holton*, 1997], temperature variance will increase as the $\bar{u} = 0$ (critical) level is approached. Nonlinear effects and dissipation will limit this growth close to the critical level, so that temperature variance will maximize below; Figure 10b shows the temperature variance maximum 1–2 km below the $\bar{u} = 0$ level.

[32] A second process that may contribute to the variance increase is that the vertical group velocity for inertia-gravity waves slows down as the waves approach a critical level ($Cg_z \sim |\bar{u} - c|^2$). For intermittent wave sources (e.g., from transient tropical convection) and "snapshot" observations (like GPS), the probability of observing wave temperature perturbations is proportional to Cg_z^{-1}, or $|\bar{u} - c|^{-2}$ [see *Alexander et al.*, 2002]. Both the intrinsic growth in temperature perturbations and the increased "observability" near the critical line may contribute to the observed behavior in Figure 10b.

[33] **Acknowledgments.** We thank Bill Kuo, Chris Rocken and Bill Schreiner for discussions regarding GPS data, and Joan Alexander, Ken Bowman, Masatomo Fujiwara, Rolando Garcia, George Kiladis, Anne Smith and Klaus Weickman for discussions and comments on the manuscript. This work is partially supported by the NASA ACMAP program. The GPS Earth Observatory group at NASA's Jet Propulsion Laboratory manages the GPS flight instruments that provided data for this study. The National Center for Atmospheric Research is sponsored by the National Science Foundation.

References

Alexander, M. J., T. Tsuda, and R. A. Vincent (2002), Latitude variations observed in gravity waves with short vertical wavelengths, *J. Atmos. Sci.*, *59*, 1394–1404.

Alexander, M. T., and J. R. Holton (1997), A model study of zonal forcing in the equatorial stratosphere by convectively induced gravity waves, *J. Atmos. Sci.*, *54*, 408–419.

Allen, S., and R. Vincent (1995), Gravity wave activity in the lower atmosphere: Seasonal and latitudinal variations, *J. Geophys. Res.*, *100*, 1327–1350.

Andrews, D. G., J. R. Holton, and C. B. Leovy (1987), *Middle Atmosphere Dynamics*, 489 pp., Elsevier, New York.

Angell, J. K., G. F. Cotton, and J. Korshover (1973), A climatological analysis of oscillations of Kelvin wave period at 50 mb, *J. Atmos. Sci.*, *30*, 13–24.

Boehm, M. T., and J. Verlinde (2000), Stratospheric influence on upper tropospheric tropical cirrus, *Geophys. Res. Lett.*, *27*, 3209–3212.

Canziani, P. O. (1999), Slow and ultraslow equatorial Kelvin waves, *Q. J. R. Meteorol. Soc.*, *125*, 657–676.

Canziani, P. O., and J. R. Holton (1998), Kelvin waves and the quasi-biennial oscillation: An observational analysis, *J. Geophys. Res.*, *103*, 31,509–31,521.

Fujiwara, M., and M. Takahashi (2001), Role of the equatorial Kelvin wave in stratosphere-troposphere exchange in a general circulation model, *J. Geophys. Res.*, *106*, 22,763–22,780.

Fujiwara, M., K. Kita, and T. Ogawa (1998), Stratosphere-troposphere exchange of ozone associated with the equatorial Kelvin wave as observed with ozonesondes and rawinsondes, *J. Geophys. Res.*, *103*, 19,173–19,182.

Fujiwara, M., F. Hasebe, M. Shiotani, N. Nishi, H. Vomel, and S. J. Oltmans (2001), Water vapor control at the tropopause by equatorial Kelvin waves observed over the Galapagos, *Geophys. Res. Lett.*, *28*, 3143–3146.

Fujiwara, M., M. K. Yamamoto, H. Hashiguchi, T. Horinouchi, and S. Fukao (2003), Turbulence at the tropopause due to breaking Kelvin waves observed by the equatorial atmosphere radar, *Geophys. Res. Lett.*, *30*(4), 1171, doi:10.1029/2002GL016278.

Garcia, R. R., and M. L. Salby (1987), Transient response to localized episodic heating in the tropics. part II: Far-field behavior, *J. Atmos. Sci.*, *44*, 499–530.

Hajj, G. A., C. O. Ao, B. A. Iijima, D. Kuang, E. R. Kursinski, A. J. Mannucci, T. K. Meehan, L. J. Romans, M. de la Torre Juarez, and T. P. Yunck (2004), CHAMP and SAC-C atmospheric occultation results and intercomparisons, *J. Geophys. Res.*, *109*, D06109, doi:10.1029/2003JD003909.

Hayashi, Y. (1982), Space-time spectral analysis and its application to atmospheric waves, *J. Meteorol. Soc. Jpn.*, *60*, 156–171.

Highwood, E. J., and B. J. Hoskins (1998), The tropical tropopause, *Q. J. R. Meteorol. Soc.*, *124*, 1579–1604.

Holton, J. R., M. J. Alexander, and M. T. Boehm (2001), Evidence for short vertical wavelength Kelvin waves in the DOE-ARM Naun99 radiosonde data, *J. Geophys. Res.*, *106*, 20,125–20,130.

Jensen, E., and L. Pfister (2004), Transport and freeze-drying in the tropical tropopause layer, *J. Geophys. Res.*, *109*, D02207, doi:10.1029/2003JD004022.

Johnson, R. H., and P. E. Ciesielski (2000), Rainfall and radiative heating rates from TOGA COARE atmospheric budgets, *J. Atmos. Sci.*, *57*, 1497–1514.

Kuang, Z., and C. S. Bretherton (2004), Convective influence on the heat balance of the tropical tropopause layer: A cloud-resolving model study, *J. Atmos. Sci.*, *61*, 2919–2927.

Kursinski, E. R., et al. (1996), Initial results of radio occultation observations of Earth's atmosphere using the Global Positioning System, *Science*, *271*, 1107–1110.

Lindzen, R. S. (1981), Turbulence and stress owing to gravity wave and tidal breakdown, *J. Geophys. Res.*, *86*, 9707–9714.

Madden, R. A., and P. R. Julian (1971), Detection of a 40–50 day oscillation in the zonal wind in the tropical Pacific, *J. Atmos. Sci.*, *28*, 702–708.

Maruyama, T. (1991), Annual and QBO-synchronized variations of lower-stratospheric equatorial wave activity over Singapore during 1961–1989, *J. Meteorol. Soc. Jpn.*, *69*, 219–232.

Mote, P. W., T. J. Dunkerton, and D. Wu (2002), Kelvin waves in stratospheric temperature observed by the Microwave Limb Sounder, *J. Geophys. Res.*, *107*(D14), 4218, doi:10.1029/2001JD001056.

Naujokat, B. (1986), An update of the observed quasi-biennial oscillation of the stratospheric winds over the tropics, *J. Atmos. Sci.*, *43*, 1873–1877.

Randel, W. J., F. Wu, and W. Rivera Rios (2003), Thermal variability of the tropical tropopause region derived from GPS/MET observations, *J. Geophys. Res.*, *108*(D1), 4024, doi:10.1029/2002JD002595.

Rocken, C., et al. (1997), Analysis and validation of GPS/MET data in the neutral atmosphere, *J. Geophys. Res.*, *102*, 29,849–29,866.

Salby, M. L., and R. R. Garcia (1987), Transient response to localized episodic heating in the tropics, 1, Excitation and short-term near-field behavior, *J. Atmos. Sci.*, *44*, 458–498.

Salby, M. L., D. L. Hartmann, P. L. Bailey, and J. C. Gille (1984), Evidence for equatorial Kelvin modes in Nimbus-7 LIMS, *J. Atmos. Sci.*, *41*, 220–235.

Sato, K., F. Hasegawa, and I. Hirota (1994), Short period disturbances in the equatorial lower stratosphere, *J. Meteorol. Soc. Jpn*, *72*, 859–872.

Seidel, D. J., R. J. Ross, J. K. Angell, and G. C. Reid (2001), Climatological characteristics of the tropical tropopause as revealed by radiosondes, *J. Geophys. Res.*, *106*, 7857–7878.

Sherwood, S. C., and A. E. Dessler (2001), A model for transport across the tropical tropopause, *J. Atmos. Sci.*, *58*, 765–779.

Sherwood, S. C., T. Horinouchi, and H. A. Zeleznik (2003), Convective impact on temperatures observed near the tropical tropopause, *J. Atmos. Sci.*, *60*, 1847–1856.

Shimizu, A., and T. Tsuda (1997), Characteristics of Kelvin waves and gravity waves observed with radiosondes over Indonesia, *J. Geophys. Res.*, *102*, 26,159–26,171.

Shiotani, M., and T. Horinouchi (1993), Kelvin wave activity and the quasi-biennial oscillation in the equatorial lower stratosphere, *J. Meteorol. Soc. Jpn.*, *71*, 175–182.

Shiotani, M., J. C. Gille, and A. E. Roche (1997), Kelvin waves in the equatorial lower stratosphere as revealed by cryogenic limb array etalon spectrometer temperature data, *J. Geophys. Res.*, *102*, 26,131–26,140.

Smith, A. K., P. Preusse, and J. Oberheide (2002), Middle atmosphere Kelvin waves observed in Cryogenic Infrared Spectrometers and Telescopes for the Atmosphere (CRISTA) 1 and 2 temperature and trace species, *J. Geophys. Res.*, *107*(D23), 8177, doi:10.1029/2001JD000577.

Straub, K. H., and G. Kiladis (2002), Observations of a convectively coupled Kelvin wave in the eastern Pacific ITCZ, *J. Atmos. Sci.*, *59*, 30–53.

Takayabu, Y. N., and M. Murakami (1991), The structure of super cloud clusters observed in 1–20 June 1986 and their relationship to easterly waves, *J. Meteorol. Soc. Jpn.*, *69*, 105–125.

Tsai, H.-F., T. Tsuda, G. Hajj, J. Wickert, and Y. Aoyama (2004), Equatorial Kelvin waves observed with GPS occultation measurements (CHAMP and SAC-C), *J. Meteorol. Soc. Jpn.*, *82*, 397–406.

Tsuda, T., Y. Murayama, H. Wiryosumarto, S. W. B. Harijono, and S. Kato (1994), Radiosonde observations of equatorial atmosphere dynamics over Indonesia: 1. Equatorial waves and diurnal tides, *J. Geophys. Res.*, *99*, 10,491–10,505.

Tsuda, T., M. Nishida, C. Rocken, and R. H. Ware (2000), A global morphology of gravity wave activity in the stratosphere revealed by the GPS occultation data (GPS/MET), *J. Geophys. Res.*, *105*, 7257–7273.

Wallace, J. M., and V. Kousky (1968), Observational evidence of Kelvin waves in the tropical stratosphere, *J. Atmos. Sci.*, *25*, 900–907.

Wheeler, M., and G. N. Kiladis (1999), Convectively coupled equatorial waves: Analysis of clouds and temperature in the wavenumber-frequency domain, *J. Atmos. Sci.*, *56*, 374–399.

Wheeler, M., G. N. Kiladis, and P. J. Webster (2000), Large-scale dynamical fields associated with convectively coupled equatorial waves, *J. Atmos. Sci.*, *57*, 613–640.

Wickert, J., et al. (2001), Atmosphere sounding by GPS radio occultation: First results from CHAMP, *Geophys. Res. Lett.*, *28*, 3263–3266.

Yang, G.-P., B. Hoskins, and J. Slingo (2003), Convectively coupled equatorial waves: A new methodology for identifying wave structures in observational data, *J. Atmos. Sci.*, *60*, 1637–1654.

W. J. Randel and F. Wu, Atmospheric Chemistry Division, NCAR, Boulder, CO 80307, USA. (randel@ucar.edu)